

Magnetoelectric antiferromagnets as platforms for the manipulation of solitons

Ricardo Zarzuela, Se Kwon Kim, and Yaroslav Tserkovnyak

Department of Physics and Astronomy, University of California, Los Angeles, California 90095, USA

(Received 18 July 2017; revised manuscript received 15 November 2017; published 17 January 2018)

We study the magnetic dynamics of magnetoelectric antiferromagnetic thin films, where an unconventional boundary ferromagnetism coexists with the bulk Néel phase below the Néel temperature. The spin exchange between the two order parameters yields an effective low-energy theory that is formally equivalent to that of a ferrimagnet. Dynamics of domain walls and skyrmions are analyzed within the collective-variable approach, from which we conclude that they behave as massive particles moving in a viscous medium subjected to a gyrotropic force. We find that the film thickness can be used as a control parameter for the motion of these solitons. In this regard, it is shown that an external magnetic field can drive the dynamics of domain walls, whose terminal velocity is tunable with the sample thickness. Furthermore, the classification of the skyrmion dynamics is sensitive to the spatial modulation of the sample thickness, which can be easily engineered with the present (thin-film) deposition techniques. Current-driven spin transfer can trigger drifting orbits of skyrmions, which can be utilized as racetracks for these magnetic textures.

DOI: [10.1103/PhysRevB.97.014418](https://doi.org/10.1103/PhysRevB.97.014418)**I. INTRODUCTION**

The magnetoelectric effect refers to the induction of bulk magnetization (electric polarization) by an electric (magnetic) field [1–3]. It requires the breaking of time-reversal symmetry, which implies the existence of a magnetic order in systems of localized spins [4], and of inversion symmetry (at the level of the magnetic point group) [2,5]. Magnetically ordered magnetoelectrics exhibit surface ferromagnetism, whose existence can be argued on symmetry grounds [6]: Broken reflection symmetry with respect to the surface allows for a Rashba electric field normal to it, which in turn induces the ferromagnetic spin density via the magnetoelectric coupling. In that regard, magnetoelectric antiferromagnets (ME-AFMs) stand out among these materials because of the following feature: There is a subclass of ME-AFMs, including α -Cr₂O₃ and Fe₂TeO₆, for which the magnetoelectric response is dominated by the exchange-driven mechanism and, strikingly, the emergent boundary magnetization is collinear with the (bulk) Néel order [7–9]. The macroscopic signatures of this unconventional surface ferromagnetism are well known experimentally [10], and the ensuing ferrimagnetic state, which is described by the staggered order parameter, offers promising perspectives to manipulate the dynamics of topological solitons [11]. The latter magnetic textures have been intensively studied in recent years due to their topological robustness (meaning that the spin texture cannot be deformed continuously into the trivial uniform state) and to their potential use as building blocks for information storage and logic devices [12,13]. Of particular interest are domain walls [14] (DWs) and skyrmions [15] due to their particlelike behavior and low current threshold for skyrmion depinning [13].

In this paper we construct a low-energy theory for ME-AFMs taking into account the aforementioned surface effects. We focus on energy terms that favor topological solitons, with special attention to DWs and skyrmions. We furthermore study

the magnetic dynamics of these two soliton classes, driven by an external magnetic field (DWs) and by an electric charge current (skyrmions), in ME-AFM thin films. In this regard, we consider the case of a quasi-two-dimensional (quasi-2D) ME-AFM film subjected to spin exchange and spin-orbit coupling with a heavy metal adjacent to one of its surfaces. In this setup, the proximate heavy metal plays two roles: First, it induces an interfacial Dzyaloshinskii-Moriya interaction, which promotes the stabilization of skyrmion textures. Second, it serves as a medium for the charge current to flow and thereby interact with the adjacent magnetic film, offering an additional knob to drive the magnetic dynamics when the magnet itself is insulating. The DW dynamics correspond, within the collective-variable approach, to that of massive particles moving in a viscous medium and subjected to a gyrotropic force depending on their precessional degree of freedom. We find that the field-driven terminal velocity of DWs shows a nonlinear behavior as a function of the sample thickness. On the other hand, the Thiele equation for skyrmions, which we derive using collective variables, is analogous to the equation of motion for a massive charged particle in a viscous medium subjected to a gyrotropic force depending on its charge. We find that these dynamics can be sustained by feasible electric currents via the spin-transfer torque effect and that the class of skyrmion trajectories realized, including drifting orbits [16,17], depends on the details of the film thickness profile. Our framework, albeit generic for ME-AFMs, will be built upon the example of chromia, α -Cr₂O₃, for illustrative purposes.

II. EFFECTIVE THEORY

Chromia represents the archetypical (insulating) ME-AFM: It is a pure (bulk) antiferromagnet, meaning that it exhibits neither weak ferromagnetism [18,19] nor magnetic (texture) superstructures [20] in the ground state below the Néel

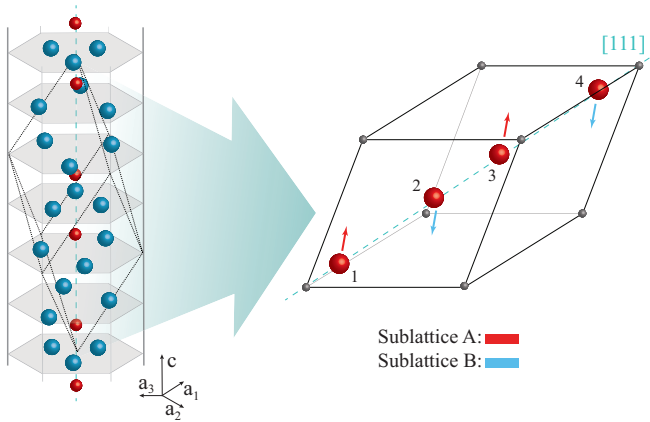


FIG. 1. Corundum-type crystal structure of eskolaite (mineral form of α - Cr_2O_3). The inset depicts the corresponding unit cell. The parameters of the rhombohedral crystal lattice are $a = 4.95 \text{ \AA}$ and $c = 13.58 \text{ \AA}$ (referred to the hexagonal frame). Red (blue) spheres represent Cr^{3+} (O^{2-}) ions. Red (sublattice A) and blue (sublattice B) arrows illustrate a spin arrangement of the Cr^{3+} ions corresponding to the antiferromagnetic phase: $s_1 = -s_2 = s_3 = -s_4$.

temperature $T_N \simeq 307 \text{ K}$. It has the (bulk) symmetry of the rhombohedral space group $R\bar{3}c$ and crystallizes in a corundum-type structure (see Fig. 1), with the unit cell containing four (crystallographically equivalent) Cr^{3+} ions located along a body diagonal of the rhombohedron. The low-energy magnetic dynamics of bulk chromia corresponds to that of an ordinary (bipartite) antiferromagnet: The two magnetic sublattices consist of Cr^{3+} ions at sites $\{1,3\}$ and $\{2,4\}$ within each unit cell (see inset of Fig. 1), and the system is magnetically described by the staggered order parameter $s_1 - s_2 + s_3 - s_4$ and the (residual) spin density $s_1 + s_2 + s_3 + s_4$ per unit cell [21].

We consider the geometry of a chromia film deposited on top of a heavy metal, with the flat interface lying along the (111) plane (see Fig. 2). Our choice of coordinate system takes the z axis along the trigonal axis, i.e., the normal to the interface. An equilibrium boundary magnetization emerges for this geometry since chromia exhibits a magnetoelectric response [6]. The heavy-metal substrate endows a Dzyaloshinskii-Moriya interaction in the antiferromagnetic film due to the breaking of the reflection symmetry with respect to the basal plane [22], which favors spin (texture) superstructures and, in particular, stabilizes skyrmion textures. Furthermore, it makes the two film surfaces become magnetically inequivalent, and as a result, a net boundary magnetization is present in the heterostructure. It is worth remarking that this effect on the ME-AFM is interfacial in nature, so that it will be enhanced (relative to the bulk) in thin films.

We regard the heterostructure as a quasi-2D system along the xy plane, which we take to be isotropic at the coarse-grained level. This approach is well suited for film thicknesses less than the DW width. An effective long-wavelength theory for bulk chromia can be developed in terms of two continuum coarse-grained fields [21], namely, the Néel order \mathbf{l} and the (volume) spin density $s\mathbf{m}$. These fields satisfy the nonlinear local constraints $\mathbf{l}^2 = 1$ and $\mathbf{l} \cdot \mathbf{m} = 0$, s represents the saturated (volume) spin density [23], and the presence of a well-developed Néel order implies $|\mathbf{m}| \ll 1$ on the scale of the

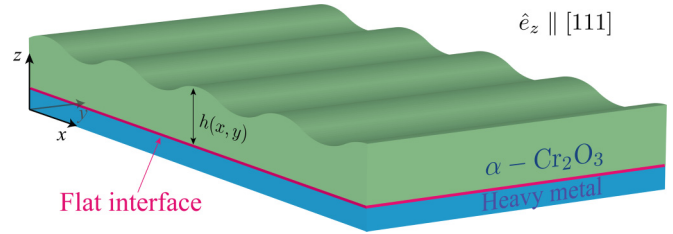


FIG. 2. Schematic of the heterostructure: A film made of chromia (α - Cr_2O_3) is deposited on top of a flat heavy-metal substrate. The film is grown along the [111] direction of its rhombohedral crystal lattice, and its thickness varies over the interface, which is described by the profile $h(x,y)$. This figure illustrates the example of a periodically modulated thickness along the x axis.

exchange coupling. In the absence of electromagnetic fields, the Lagrangian density for bulk chromia in the continuum limit becomes

$$\mathcal{L}_{\text{bulk}}[t; \mathbf{l}, \mathbf{m}] = s \mathbf{m} \cdot (\mathbf{l} \times \partial_t \mathbf{l}) - \frac{m^2}{2\chi_{\perp}} - \mathcal{F}_{\text{stag}}[\mathbf{l}] \quad (1)$$

to the lowest order (quadratic) in both $\partial_t \mathbf{l}$ and \mathbf{m} [24]. The first term is the kinetic Lagrangian, which originates in the accumulation of geometric Berry phases from individual spins and establishes the canonical conjugacy between the Néel order and the spin density since the canonical momentum reads $\Pi_{\mathbf{l}} = s \mathbf{m} \times \mathbf{l}$ [25]. Furthermore, χ_{\perp} denotes the transverse spin susceptibility, and $\mathcal{F}_{\text{stag}}[\mathbf{l}]$ stands for the effective energy for the Néel order, whose minimal model contains (bulk) isotropic exchange, (bulk) uniaxial anisotropy, and (interfacial) Dzyaloshinskii-Moriya contributions [26]:

$$\mathcal{F}_{\text{stag}}[\mathbf{l}] = \frac{A}{2} \sum_{\mu=1,2} (\partial_{x_{\mu}} \mathbf{l})^2 + \frac{1}{2} K l_z^2 + D(\mathbf{l} \cdot \nabla l_z - l_z \nabla \cdot \mathbf{l}), \quad (2)$$

where A and K are the (exchange) stiffness and anisotropy constants, respectively, and D denotes the strength of the Dzyaloshinskii coupling. $K < 0$ describes the hard (anisotropy) xy plane, and both A and χ^{-1} are proportional to $J S^2$, where J is the microscopic exchange energy. The model is minimal in the sense that it contains all symmetry-allowed exchange and relativistic energy terms up to second order in the Néel order and its spatial derivatives. Note that bulk Dzyaloshinskii-Moriya terms are forbidden by the centrosymmetry of $R\bar{3}c$, the space group of chromia [20]. Integration out of the spin field \mathbf{m} yields the following effective Lagrangian density for the Néel order:

$$\mathcal{L}_{\text{bulk,eff}}[t; \mathbf{l}] = \frac{1}{2} s^2 \chi (\partial_t \mathbf{l})^2 - \mathcal{F}_{\text{stag}}[\mathbf{l}], \quad (3)$$

where the first term accounts for the inertia of the dynamics of the Néel order.

The boundary spin density $s\mathbf{m}_b$ describes the spin-polarized state at the chromia/heavy-metal interface, where s is the uncompensated (surface) spin density [27]. It contributes to the effective theory with a 2D Lagrangian density of the form

$$\mathcal{L}_{\text{surf}}[t; \mathbf{l}, \mathbf{m}_b] = \mathcal{L}_{\text{WZ}}[\mathbf{m}_b, \partial_t \mathbf{m}_b] - \mathcal{F}_{\text{surf}}[\mathbf{l}, \mathbf{m}_b], \quad (4)$$

where the first term corresponds to the Wess-Zumino action of the (2+1)-dimensional field theory of ferromagnetism [28],

$\mathcal{L}_{\text{WZ}}[\mathbf{m}_b, \partial_t \mathbf{m}_b] = -\mathbf{s} \mathbf{a}[\mathbf{m}_b] \cdot \partial_t \mathbf{m}_b$. Here, $\mathbf{a}[\mathbf{x}]$ is the vector potential for the magnetic monopole [29], $\nabla_x \times \mathbf{a} = \mathbf{x}$, and $\mathcal{F}_{\text{surf}}[\mathbf{l}, \mathbf{m}_b]$ stands for the 2D free-energy density associated with the boundary magnetization. It is worth recalling here that chromia exhibits a spin-exchange-driven magnetoelectric response at not too low temperatures [30,31]. Phenomenologically, this means that an applied electric field induces a shift in the intralattice exchange constants of the form $J_{AA} \rightarrow J_{AA} + \delta J$ and $J_{BB} \rightarrow J_{BB} - \delta J$, which, in turn, engenders an enhancement or reduction of the sublattice spin polarizations compared to those of the compensated (zero-field) case. As a result, the magnetoelectric effect produces a net boundary magnetization $\mathbf{s} \mathbf{m}_b$ that is collinear with the staggered order parameter regardless of their orientation. A minimal model for the energy density for the magnetization at the interface reads

$$\mathcal{F}_{\text{surf}}[\mathbf{l}, \mathbf{m}_b] = \frac{m_b^2}{2\chi_{\parallel}^b} - \eta \mathbf{m}_b \cdot \mathbf{l}, \quad (5)$$

where χ_{\parallel}^b is the longitudinal spin susceptibility at the interface and η is the coupling constant for the exchange-driven magnetoelectric effect. We have disregarded higher-order terms in the boundary magnetization and up to second-order terms in $\nabla \mathbf{m}_b$ (exchange and relativistic) since the exchangelike coupling $\propto \mathbf{m}_b \cdot \mathbf{l}$ dominates the energetics at the interface. This term establishes the collinearity between both order parameters, as can easily be seen from minimization of the functional with respect to \mathbf{m}_b . Integration out of the boundary magnetization yields, to the leading order in the staggered order parameter, the following effective 2D Lagrangian density for the heterostructure [32]:

$$\mathcal{L}_{\text{eff}}[t; \mathbf{l}] = -\mathbf{s} \mathbf{a}[\mathbf{l}] \cdot \partial_t \mathbf{l} + \frac{\rho}{2} (\partial_t \mathbf{l})^2 - \mathcal{F}[\mathbf{l}], \quad (6)$$

where $\rho = s^2 \chi h$ and $\mathcal{F} = h \mathcal{F}_{\text{stag}} + \mathcal{F}_{\text{surf}}$ are the effective inertia and (total) free-energy densities, respectively, and $h(x, y)$ denotes the 2D thickness profile of the chromia film.

The effects of an external magnetic field can be incorporated into our effective theory as follows: First, we consider here the exchange approximation, in which the Lagrangian density is assumed to be invariant under the global spin rotations. By doing so we neglect relativistic interactions, which break this symmetry, by treating them as a perturbation, in the spirit of Ref. [33]. Second, the net spin density (i.e., the conserved Noether charge associated with the symmetry of the Lagrangian under global spin rotations) reads $\mathbf{s} = \mathbf{s} \mathbf{l} + \rho \mathbf{l} \times \partial_t \mathbf{l}$. In the presence of an external magnetic field \mathbf{H} , the total magnetization can be cast as $\mathbf{M} = g \mathbf{s} \mathbf{l} + g \rho \mathbf{l} \times \partial_t \mathbf{l} + \hat{\chi}^* \mathbf{H}$, where g denotes the gyromagnetic ratio and $\hat{\chi}^*$ is the magnetic susceptibility tensor. Since $\mathbf{M} = \partial \mathcal{L}_{\text{eff}} / \partial \mathbf{H}$, the susceptibility must take the form $\chi_{ij}^* = \rho g^2 (1 - l_i l_j)$, and therefore, the effective Lagrangian density is extended to

$$\mathcal{L}_{\text{eff}}[t; \mathbf{l}] = -\mathbf{s} \mathbf{a}[\mathbf{l}] \cdot \partial_t \mathbf{l} + \frac{\rho}{2} (\partial_t \mathbf{l} - g \mathbf{l} \times \mathbf{H})^2 - \mathcal{F}[\mathbf{l}], \quad (7)$$

where $\mathcal{F}[\mathbf{l}]$ now includes the Zeeman term $-g \mathbf{s} \mathbf{l} \cdot \mathbf{H}$ [34]. To conclude this section, dissipation can be incorporated phenomenologically into our heterostructure via the dissipative Gilbert-Rayleigh function, $\mathcal{R}[\mathbf{l}] = h s \alpha (\partial_t \mathbf{l})^2 / 2$, which is half of the dissipation power density. Here, α denotes the bulk Gilbert-damping constant, which can be attributed to, for

example, magnon-phonon interactions, and we have omitted the interface contribution to dissipation [35]. Henceforth, we will treat chromia as a ferrimagnet and study the ensuing dynamics of DWs and skyrmions, bearing in mind the film thickness as a control parameter. Note that this approach differs from previous studies based on the thermal and/or chemical control of the saturated spin density [36].

III. DOMAIN WALL DYNAMICS

We consider in what follows magnetic solitons whose dynamics are encoded in the time evolution of a discrete set of soft modes (collective-variable description). Of particular interest are DWs [14], which can be described by their center of mass X and azimuthal angle Φ in the low-frequency (compared to the exchange energy) regime. Let x denote the direction of the DW propagation and h be uniform. Accounting for the ansatz $\cos \Theta(x) = \tanh[(x - X)/\delta]$ for the out-of-plane component of the Néel order in the spherical-coordinate representation, $\mathbf{l} = (\sin \Theta \cos \Phi, \sin \Theta \sin \Phi, \cos \Theta)$, the Euler-Lagrange equations for the Lagrangian density (7) become [32]

$$2\delta s \dot{\Phi} + 2\rho \ddot{X} + 2s\alpha h \dot{X} = \delta F_X, \quad (8)$$

$$-2s \dot{X} + 2\delta \rho \ddot{\Phi} + 2\delta s\alpha h \dot{\Phi} = F_{\Phi}, \quad (9)$$

where $F_X = -\delta_X F$ and $F_{\Phi} = -\delta_{\Phi} F$ are the thermodynamic forces conjugate to X and Φ , respectively, with F being the total free energy. Here, the DW width is given by $\delta = \sqrt{A/|K|}$.

In the presence of a strong magnetic field, $\mathbf{H} = H_z \hat{e}_z$, the energetics of the ME-AFM are dominated by the Zeeman coupling, so that the thermodynamic forces can be approximated by $F_X \simeq -2g s H_z$ and $F_{\Phi} \simeq 0$. Equation (9) therefore dictates that $\dot{\Phi}|_{\text{st}} = \mathbf{s}(\dot{X}|_{\text{st}})/\delta s\alpha h$ is the angular velocity of the DW in the steady state. By substituting it into Eq. (8) we obtain the following expression for the field-driven terminal velocity of the DW:

$$V = \frac{2h/h_{\star}}{1 + (h/h_{\star})^2} V_{\text{max}}, \quad (10)$$

where $h_{\star} = s/\alpha$ and $V_{\text{max}} = g\delta H_z/2$ is the maximum velocity. Its reduction compared to V_{max} is due to the ferromagnetic nature of the surface, and h/h_{\star} parametrizes the effective damping α_{eff} . Since the usual DW terminal velocity is $\propto \alpha_{\text{eff}}/(1 + \alpha_{\text{eff}}^2)$ [14], we obtain a maximum at the value $h = h_{\star}$ of the film thickness (see Fig. 3). In summary, the DW velocity can be tuned by both the external magnetic field and the film thickness, with the latter being responsible for the nonlinear behavior.

IV. SKYRMION DYNAMICS

Skyrmions are the epitome of spatially localized solitons in two dimensions [15], exhibit topological charge, and arise in magnetic systems with spin-orbit coupling [37]. For the free-energy model (2), skyrmions are stabilized with the energy $\mathcal{F}_{\text{sky}} \propto 4\pi A|Q|$ and the characteristic length scale $R_{\star} = 2\pi D/|K|$ for the skyrmion radius [38]. These spin textures can be described, using collective coordinates, by their center of mass $\mathbf{X} = (X, Y)$ in the low-frequency (compared to the exchange energy) regime. Since details of their geometry (shape) are encoded in hard modes of the texture,

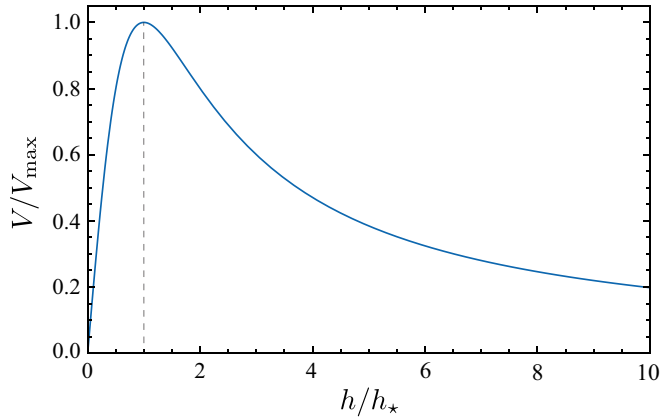


FIG. 3. Dependence of the field-driven terminal velocity of the domain wall on the thickness of the ME-AFM film. Both quantities have been normalized to the maximum velocity $V_{\max} = g\delta H_z/2$ and the length scale $h_* = s/s\alpha$. The dashed line illustrates the maximum of the terminal velocity reached at the value $h = h_*$ of the film thickness.

we can take skyrmions to be rigid in the spirit of our low-frequency long-wavelength treatment. Taking into account the ansatz $\mathbf{l}[t, \mathbf{r}] = \mathbf{l}_0[\mathbf{r} - \mathbf{X}(t)]$ for the order parameter, the Euler-Lagrange equations for the Lagrangian density (6) now become

$$\rho_M h(\mathbf{X}) \ddot{\mathbf{X}} + 4\pi s \mathcal{Q} \dot{\mathbf{X}} \times \hat{e}_z + \Gamma h(\mathbf{X}) \dot{\mathbf{X}} = \mathbf{F}_{\text{int}} + \mathbf{F}_J, \quad (11)$$

where the terms on the left-hand side represent (from left to right) the inertial, Magnus, and friction forces acting on the skyrmion, respectively. Here, $\rho_M = s^2 \chi \int_{\mathbf{R}^2} dx dy (\partial_x \mathbf{l}_0)^2$ is the inertia density (per thickness), $\Gamma = \alpha \rho_M / \chi s$ denotes the viscous coefficient, and $\mathcal{Q} = \int_{\mathbf{R}^2} dx dy \mathbf{l}_0 \cdot (\partial_x \mathbf{l}_0 \times \partial_y \mathbf{l}_0) / 4\pi$ is the Pontryagin index (so-called topological charge) of the skyrmion texture, which is a topological invariant and provides a measure of the wrapping of the order parameter $\mathbf{l}_0(\mathbf{r})$ around the unit sphere.

Our Thiele equation [39] for the soft modes, Eq. (11), is derived within the linear-response approach for the case of thickness profiles $h(x, y)$ smooth over length scales larger than the typical size of the skyrmion. This requirement translates into the adiabatic condition $|\partial_{x,y} \ln h| R_* \ll 1$. Finally, $\mathbf{F}_{\text{int}} = -\delta_X F$ is the conservative force, and \mathbf{F}_J represents the force exerted on the skyrmion by a charge current \mathbf{J} flowing in the heavy-metal substrate. The latter stems from the spin-transfer torque exerted on the spin texture by the applied charge current via the (exchange) proximity effect [40] and takes the form $F_{J,i} := \int_{\mathbf{R}^2} dx dy \{ \zeta_1 \mathbf{l}_0 \cdot [(\mathbf{J} \cdot \nabla) \mathbf{l}_0 \times \partial_i \mathbf{l}_0] - \zeta_2 \partial_i \mathbf{l}_0 \cdot (\mathbf{J} \cdot \nabla) \mathbf{l}_0 \}$, $i = x, y, z$, where ζ_1 and ζ_2 are the phenomenological constants for the reactive and dissipative components of the spin-transfer torque, respectively [36]. For a spatially constant (therefore divergenceless) charge current, $\mathbf{J} = J_x \hat{e}_x + J_y \hat{e}_y$, we can recast these identities as the linear system

$$\begin{pmatrix} F_{J,x} \\ F_{J,y} \end{pmatrix} = \begin{pmatrix} -\frac{\rho_M}{\chi s^2} \zeta_2 & -4\pi \mathcal{Q} \zeta_1 \\ 4\pi \mathcal{Q} \zeta_1 & -\frac{\rho_M}{\chi s^2} \zeta_2 \end{pmatrix} \begin{pmatrix} J_x \\ J_y \end{pmatrix}. \quad (12)$$

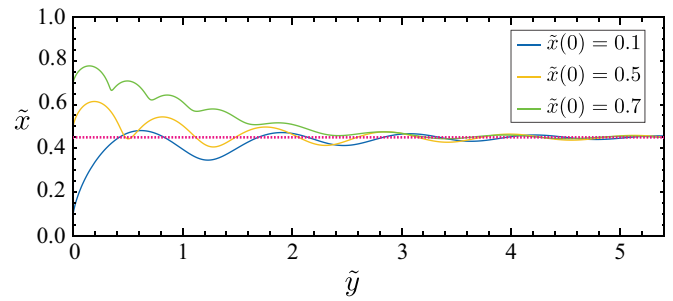


FIG. 4. Driftinglike orbits of skyrmions with topological charge $\mathcal{Q} = 1$ subjected to the current-induced force $\tilde{\mathbf{F}}_J = 0.8(4\pi \hat{e}_x + \mathcal{K} \hat{e}_y)$ for the hyperbolic thickness profile $h(\tilde{x})/\mathcal{T} = 1 + 0.7 \tanh[10(\tilde{x}_c - \tilde{x})]$, with $\tilde{x}_c = 0.45$. These trajectories are calculated by numerical integration of the dimensionless equations of motion (14) with the following values of the parameters: $\mathcal{K} = 0.9\pi$ and $4\pi s/\alpha s \mathcal{T} = 4\pi$. In the calculations we have taken the initial velocity $\dot{\tilde{x}}(0) = \dot{\tilde{y}}(0) = 0$ and initial position along the x axis [$\tilde{y}(0) = 0$]: $\tilde{x}(0) = 0.1$ (blue), $\tilde{x}(0) = 0.5$ (yellow), and $\tilde{x}(0) = 0.7$ (green). The magenta dashed line at $\tilde{x} = \tilde{x}_c$ depicts the (attractive) racetrack for the skyrmion dynamics.

Since its determinant is nonzero, the current-to-force conversion is a bijective map, which means that we can generate any (spatially constant) current-induced force profile. On the other hand, spin-orbit torques do not exert an effective force on the skyrmion texture for the rigid ansatz [41]. Henceforth, we will assume the lowest-energy configuration for these solitons (corresponding to the charge $\mathcal{Q} = \pm 1$) and focus on their current-driven dynamics by disregarding the internal force.

We consider the simple scenario of one-dimensional thickness profiles (along a direction defined as the x axis), $h \equiv h(x)$. As a specific illustrative example, we study the linear profile $h(x) = \mathcal{T} - h_0 x/L$, where L is the lateral size of the chromia film (spanning the domain $0 \leq x \leq L$) and the heights h_0, \mathcal{T} satisfy the conditions $h_0 < \mathcal{T}$ and $h_0 R_*/L \ll \mathcal{T}$. In the steady state, solutions of Eq. (11) are given by

$$\dot{\mathbf{X}} = \frac{1}{16\pi^2 s^2 + \Gamma^2 h^2(X)} \begin{pmatrix} \Gamma h(X) F_{J,x} - 4\pi s \mathcal{Q} F_{J,y} \\ 4\pi s \mathcal{Q} F_{J,x} + \Gamma h(X) F_{J,y} \end{pmatrix}. \quad (13)$$

Let us now apply a current-induced force $\mathbf{F}_J \propto 4\pi s \mathcal{Q} \hat{e}_x + \Gamma h(X_c) \hat{e}_y$, parametrized by a certain intermediate position $0 < X_c < L$, with a positive proportionality constant. The components of the terminal velocity (13) read $V_x \propto 4\pi s \mathcal{Q} \Gamma [h(X) - h(X_c)]$ and $V_y > 0$. Therefore, since $V_x(X \leq X_c) \geq 0$, the line $x = X_c$ becomes an attractor for the dynamics of skyrmions with a topological charge \mathcal{Q} . The linear case illustrates the following general statement: Given any one-dimensional thickness profile monotonically decreasing along the (so-defined) x axis, we can generate a self-focusing skyrmion racetrack transversal to any x coordinate by tuning the current-induced force.

We illustrate this statement by performing the numerical calculation of skyrmion trajectories in the xy plane. Figure 4 depicts the generation, for a hyperbolically decreasing thickness profile, of a self-focusing skyrmion racetrack sustained by the appropriate current-induced force. The numerical

trajectories are obtained by integrating the dimensionless form of Eq. (11):

$$\mathcal{K} \frac{h(\tilde{X})}{\mathcal{T}} \left[\frac{d^2 \tilde{X}}{d\tilde{t}^2} + \frac{d\tilde{X}}{d\tilde{t}} \right] + \frac{4\pi s Q}{\alpha s \mathcal{T}} \frac{d\tilde{X}}{d\tilde{t}} \times \hat{e}_z = \tilde{F}_J, \quad (14)$$

where space and time are rescaled with respect to the lateral size L and the relaxation time $\tau = \chi s / \alpha$, respectively, and $\mathcal{K} = \int_{\mathbf{R}^2} dx dy (\partial_x I_0)^2$ denotes a (dimensionless) geometric factor determined by the skyrmion texture.

V. DISCUSSION

We have shown that ME-AFMs offer an attractive platform to control fast antiferromagnetic dynamics of DWs, driven by an external magnetic field, as in their ferrimagnetic counterparts [42]. Similar dynamics could also be triggered by an applied charge current, which exerts a force on the DW via the spin-transfer effect. The latter contributes to the equations of motion (8) and (9) two components, $F_{J,x}$ and $F_{J,\phi}$, of the total force, respectively [43]. Therefore, expression (10) for the terminal velocity of the DW is still valid upon redefinition of the maximum velocity, $V_{\max}(h) = [\delta F_{J,x} - (h_*/h) F_{J,\phi}] / 4s$, which now becomes thickness dependent. For moderate magnetic fields, Dzyaloshinskii-Moriya interactions could become relevant and contribute to the DW dynamics with $F_\phi = \pi D \sin \Phi$, which translates into an extra contribution to the maximum velocity given by the substitution $F_{J,\phi} \rightarrow F_{J,\phi} + \pi D \sin \Phi$. Accounting for the values $A \sim 10^{-11}$ J/m, $K \sim 2 \times 10^4$ J/m³, and $\alpha \sim 10^{-3}$ for the case of chromia [32,44], we estimate the DW width to be $\delta \sim 20$ nm and the maximum velocity V_{\max} to lie in the vicinity of 20 m/s for an applied magnetic field $\mu_0 H_z = 0.01$ T. Furthermore, the optimal film thickness is found to be $h_* \sim 300$ nm, which means that the terminal velocity can be increased monotonically with the thickness up to the submicrometric scale, where the Walker breakdown occurs. It is important to mention that the emergent ferromagnetism studied in Ref. [32] is a bulk property of chromia, which is controlled by an external electric field. As a result, the corresponding field-driven terminal velocity of the DW is insensitive to the sample thickness, unlike the present case.

Regarding skyrmions, the theory presented in this paper is, in a way, complementary to that of Ref. [36] for ferrimagnets since both share the same Thiele equation for the dynamics of skyrmions but have different control variables: In our case, the thickness profile plays this role through the inertia and the viscous coefficient, whereas in the ferrimagnetic case it is given by the saturated spin density of the system. That being said, our framework for the manipulation of skyrmion textures can be more advantageous for several reasons: First, from an engineering perspective, an accurate shaping of the sample

surface is more feasible than the thermal or chemical control of the saturated spin density required in Ref. [36]. Second, ferrimagnetic materials behave effectively as ferromagnets in almost all circumstances, the only exception being when (a region of) the system is driven into the (angular momentum) compensation point, where they exhibit an antiferromagnetic behavior. On the contrary, bulk ME-AFMs are intrinsically antiferromagnetic, with the ferrimagnetic character emerging in the so-called holographic fashion (it is encoded in the boundaries of the system) [45]; the ensuing dynamics are therefore suitable to be exploited in the context of antiferromagnetic spintronics. Furthermore, the exchange-driven collinearity between the boundary magnetization and the bulk Néel order allows the imaging of (the dynamics of) antiferromagnetic textures by means of magneto-optical techniques.

Our Thiele equation for skyrmions, Eq. (11), relies on the assumption of smoothness of the thickness profile. In the case of ultrathin films with a small number of layers, however, variations in the film thickness will be discrete rather than continuous. Bearing in mind our scenario of one-dimensional thickness profiles, the n -layer variation can be modeled by $\Delta h(x, y) = n \Theta[x - x_0(y)]$, where $x_0(y)$, a function of the transverse coordinate y , describes the x point at which the thickness varies abruptly. It is a fair assumption to consider $x_0(y)$ (the so-called n -layer variation front) to be randomly distributed, so that the one-dimensional n -layer variation becomes $\overline{\Delta h}(x) = n \langle \Theta[x - x_0(y)] \rangle_{\text{front}}$, where $\langle \dots \rangle_{\text{front}}$ denotes the average over realizations of the front. This procedure will typically smooth the spatial dependence of the n -layer variation, making the thickness profile $h(x)$ satisfy the adiabatic condition since $|\partial_x h|$ will be moderate close to the points of “discontinuity.” In any case, we only need the conditions $h(x > x_0) \geq h(x_0)$ and $h(x < x_0) \leq h(x_0)$ to be satisfied around a point x_0 for the skyrmion racetrack principle to work, regardless of the smoothness of the thickness profile: From Eq. (13) we conclude that self-focusing skyrmion trajectories are a steady property of the system, i.e., independent of the inertia term. On the contrary, the transient regime of the skyrmion dynamics will depend sensitively on the nature of the thickness profile.

ACKNOWLEDGMENTS

We thank O. Tchernyshyov for insightful remarks and P. Upadhyaya for drawing our attention to this class of magnetic materials. This work has been supported by the NSF-funded MRSEC under Grant No. DMR-1420451 and by the Army Research Office under Contract No. W911NF-14-1-0016. R.Z. thanks Fundación Ramón Areces for support through a post-doctoral fellowship within the XXVII Convocatoria de Becas para Ampliación de Estudios en el Extranjero en Ciencias de la Vida y de la Materia.

- [1] P. Curie, *J. Phys. (Paris)* **3**, 393 (1894).
 [2] I. E. Dzyaloshinskii, *Sov. Phys. JETP* **10**, 628 (1960).
 [3] D. N. Astrov, *Sov. Phys. JETP* **11**, 708 (1960); **13**, 729 (1961); V. J. Follen, G. T. Rado, and E. W. Stalder, *Phys. Rev. Lett.* **6**, 607 (1961).

- [4] L. D. Landau, E. M. Lifshitz, and L. P. Pitaevskii, *Electrodynamics of Continuous Media*, 2nd ed., Course of Theoretical Physics Vol. 8 (Butterworth-Heinemann, Oxford, 1984).
 [5] H. Schmid, *J. Phys. Condens. Matter* **20**, 434201 (2008).

- [6] A. F. Andreev, *JETP Lett.* **63**, 758 (1996); K. D. Belashchenko, *Phys. Rev. Lett.* **105**, 147204 (2010).
- [7] X. He, Y. Wang, N. Wu, A. N. Caruso, E. Vescovo, K. D. Belashchenko, P. A. Dowben, and Ch. Binek, *Nat. Mater.* **9**, 579 (2010).
- [8] J. L. Wang, J. A. Colon Santana, N. Wu, C. Karunakaran, J. Wang, P. A. Dowben, and Ch. Binek, *J. Phys. Condens. Matter* **26**, 055012 (2014).
- [9] L. Fallarino, A. Berger, and C. Binek, *Phys. Rev. B* **91**, 054414 (2015).
- [10] N. Wu, X. He, A. L. Wysocki, U. Lanke, T. Komesu, K. D. Belashchenko, Ch. Binek, and P. A. Dowben, *Phys. Rev. Lett.* **106**, 087202 (2011); W. Echtenkamp and Ch. Binek, *ibid.* **111**, 187204 (2013); S. Cao, X. Zhang, N. Wu, A. T. N'Diaye, G. Chen, A. K. Schmid, X. Chen, W. Echtenkamp, A. Enders, Ch. Binek, and P. A. Dowben, *New J. Phys.* **16**, 073021 (2014); L. Fallarino, A. Berger, and Ch. Binek, *Appl. Phys. Lett.* **104**, 022403 (2014).
- [11] A. Kosevich, B. Ivanov, and A. Kovalev, *Phys. Rep.* **194**, 117 (1990), and references therein.
- [12] S. S. P. Parkin, M. Hayashi, and L. Thomas, *Science* **320**, 190 (2008); A. Fert, V. Cros, and J. Sampaio, *Nat. Nanotechnol.* **8**, 152 (2013); Y. Zhou and M. Ezawa, *Nat. Commun.* **5**, 4652 (2014).
- [13] N. Nagaosa and Y. Tokura, *Nat. Nanotechnol.* **8**, 899 (2013), and references therein.
- [14] N. L. Schryer and L. R. Walker, *J. Appl. Phys.* **45**, 5406 (1974).
- [15] A. A. Belavin and A. M. Polyakov, *JETP Lett.* **22**, 245 (1975).
- [16] J. E. Müller, *Phys. Rev. Lett.* **68**, 385 (1992).
- [17] R. Menne and R. R. Gerhardts, *Phys. Rev. B* **57**, 1707 (1998); S. D. M. Zwerschke, A. Manolescu, and R. R. Gerhardts, *ibid.* **60**, 5536 (1999).
- [18] I. E. Dzyaloshinskii, *Sov. Phys. JETP* **5**, 1259 (1957).
- [19] T. Moriya, *Phys. Rev.* **120**, 91 (1960).
- [20] I. E. Dzyaloshinskii, *Sov. Phys. JETP* **19**, 960 (1964).
- [21] Chromia is a four-sublattice antiferromagnet and therefore should be generically described by three staggered order parameters: $\mathbf{L}_1 = \mathbf{s}_1 - \mathbf{s}_2 + \mathbf{s}_3 - \mathbf{s}_4$, $\mathbf{L}_2 = \mathbf{s}_1 + \mathbf{s}_2 - \mathbf{s}_3 - \mathbf{s}_4$, and $\mathbf{L}_3 = \mathbf{s}_1 - \mathbf{s}_2 - \mathbf{s}_3 + \mathbf{s}_4$. The latter two are identically zero in the uniform ground state, $\mathbf{L}_2 = \mathbf{L}_3 \equiv \mathbf{0}$ [18]. The group symmetry of chromia allows for Lifshitz invariants in the total free energy that couple \mathbf{L}_2 and \mathbf{L}_3 to spatial variations of the Néel order \mathbf{L}_1 . Therefore, in the presence of (spatially) smooth Néel textures, the other two order parameters acquire small relativistic values (compared to the Néel order) at the level of energetics. Regarding the magnetic dynamics, the dominant kinetic term in the Lagrangian description of chromia is given by the Berry-phase Lagrangian $\propto \mathbf{M} \cdot (\mathbf{L}_1 \times \partial_t \mathbf{L}_1)$ since $\mathbf{M} = \mathbf{s}_1 + \mathbf{s}_2 + \mathbf{s}_3 + \mathbf{s}_4$ is the generator of rotations; Berry-phase terms related to \mathbf{L}_2 and \mathbf{L}_3 contribute at subleading order to these dynamics. Integration out of the spins fields \mathbf{M} , \mathbf{L}_2 , and \mathbf{L}_3 leads to corrections at the (sub)subleading order to the Lagrangian (6) and therefore are usually disregarded. This yields the effective dynamical description of chromia as a bipartite antiferromagnet.
- [22] R. Zarzuela and Y. Tserkovnyak, *Phys. Rev. B* **95**, 180402 (2017).
- [23] It reads $s = \hbar S/\mathcal{V}$, where S and \mathcal{V} are the (dimensionless) spin and volume per site, respectively.
- [24] A. Auerbach, *Interacting Electrons and Quantum Magnetism* (Springer, New York, 1994); S. Sachdev, *Quantum Phase Transitions* (Cambridge University Press, Cambridge, 1999).
- [25] E. Fradkin and M. Stone, *Phys. Rev. B* **38**, 7215(R) (1988).
- [26] A longitudinal (with respect to the Néel order) component of the bulk spin density \mathbf{m}_l arises in the presence of an external electric field, which is rooted in the exchange-driven magnetoelectric effect. This adds two extra contributions to the energy model (2), $\mathbf{m}_l^2/2\chi_{\parallel} - \eta(E)\mathbf{m}_b \cdot \mathbf{l}$, where χ_{\parallel} is the longitudinal spin susceptibility of the ME-AFM and the last term represents the magnetoelectric coupling, with $\eta(E)$ being linear in the electric field.
- [27] This coarse-grained field may be defined (modulo normalization) by $\sum_{\mathbf{r}_i \in \mathcal{S}} \mathbf{S}_i \delta^{(2)}(\mathbf{r} - \mathbf{r}_i)$, where i runs over all (lattice) sites belonging to the interface \mathcal{S} between the film and the heavy metal and \mathbf{r}_i and \mathbf{S}_i are the position and spin vectors at the i th site, respectively.
- [28] G. E. Volovik, *J. Phys. C* **20**, L83 (1987).
- [29] B. Ivanov and A. Sukstanskii, *Solid State Commun.* **50**, 523 (1984); D. Loss, D. P. DiVincenzo, and G. Grinstein, *Phys. Rev. Lett.* **69**, 3232 (1992).
- [30] O. F. de Alcantara Bonfim and G. A. Gehring, *Adv. Phys.* **29**, 731 (1980).
- [31] M. Mostovoy, A. Scaramucci, N. A. Spaldin, and K. T. Delaney, *Phys. Rev. Lett.* **105**, 087202 (2010); S. Mu, A. L. Wysocki, and K. D. Belashchenko, *Phys. Rev. B* **89**, 174413 (2014).
- [32] K. D. Belashchenko, O. Tchernyshyov, A. A. Kovalev, and O. A. Tretiakov, *Appl. Phys. Lett.* **108**, 132403 (2016).
- [33] A. F. Andreev and V. I. Marchenko, *Sov. Phys. Usp.* **23**, 21 (1980).
- [34] This form of the Lagrangian can be derived, alternatively, by including a Zeeman term in the free energy (2) and integrating out the spin field \mathbf{m} and by including the corresponding Zeeman term in our theory for surface ferromagnetism [see Eq. (5)].
- [35] We focus on this case for the sake of simplicity. In general, we should include a boundary contribution $\propto \alpha_b (\partial_t \mathbf{l})^2/2$ to the Gilbert-Rayleigh dissipation function, with α_b being the boundary Gilbert-damping constant. We can account for this term by redefining the thickness profile function as $h \Rightarrow h' = h + \alpha_b/\alpha_a$ in Eqs. (10) and (13).
- [36] S. K. Kim, K.-J. Lee, and Y. Tserkovnyak, *Phys. Rev. B* **95**, 140404(R) (2017).
- [37] S. Mülbauer *et al.*, *Science* **323**, 915 (2009); S. Seki, X. Z. Yu, S. Ishiwata, and Y. Tokura, *ibid.* **336**, 198 (2012); W. Jiang *et al.*, *ibid.* **349**, 283 (2015).
- [38] H. Ochoa, S. K. Kim, and Y. Tserkovnyak, *Phys. Rev. B* **94**, 024431 (2016).
- [39] A. A. Thiele, *Phys. Rev. Lett.* **30**, 230 (1973).
- [40] K. M. D. Hals, Y. Tserkovnyak, and A. Brataas, *Phys. Rev. Lett.* **106**, 107206 (2011).
- [41] S.-Z. Lin, *Phys. Rev. B* **96**, 014407 (2017).
- [42] T. Tono, T. Taniguchi, K.-J. Kim, T. Moriyama, A. Tsukamoto, and T. Ono, *Appl. Phys. Express* **8**, 073001 (2015); K.-J. Kim *et al.*, *Nat. Mater.* **16**, 1187 (2017).

- [43] G. Tatara and H. Kohno, [Phys. Rev. Lett.](#) **92**, 086601 (2004).
- [44] The presence of the heavy-metal substrate can significantly increase the value of α ; see Ref. [46]. Therefore, we take this value of the Gilbert-damping constant to be a lower bound.
- [45] L. Susskind, [J. Math. Phys.](#) **36**, 6377 (1995); J. M. Maldacena, [Adv. Theor. Math. Phys.](#) **2**, 231 (1998).
- [46] Y. Tserkovnyak, A. Brataas, and G. E. W. Bauer, [Phys. Rev. Lett.](#) **88**, 117601 (2002).